Z. Phys. C – Particles and Fields 49, 29–41 (1991)

Zeitschrift für Physik C Particles and Fields


# A comparison of measured jet cross sections with QCD calculations for $e^+e^-$ annihilation

JADE-Collaboration

N. Magnussen[1,i], L. Smolik[3,e], J. Allison[5], K. Ambrus[3,b], R.J. Barlow[5], W. Bartel[1], S. Bethke[3], C.K. Bowdery[4], S.L. Cartwright[7,c], J. Chrin[5], D. Clarke[7], A. Dieckmann[3], I.P. Duerdoth[5], G. Eckerlin[3], E. Elsen[3,e], R. Felst[1], A.J. Finch[4], F. Foster[4], T. Greenshaw[2], J. Hagemann[2,a], D. Haidt[1], J. Heintze[3], G. Heinzelmann[2], K.H. Hellenbrand[3,d], P. Hill[6,e], G. Hughes[4], H. Kado[1,f], K. Kawagoe[8], C. Kleinwort[2,a], G. Knies[1], T. Kobayashi[8], S. Komamiya[3,g], H. Krehbiel[1], J. v. Krogh[3], M. Kuhlen[2,h], F.K. Loebinger[5], A.A. Macbeth[5], R. Marshall[7], T. Mashimo[8], R. Meinke[1], H. Meyer[1,i], R.P. Middleton[7], P.G. Murphy[5], B. Naroska[2], M. Nozaki[8], J.M. Nye[4,j], J. Olsson[1], F. Ould-Saada[2], D.D. Pitzl[2,k], R. Ramcke[1,m], H. Rieseberg[3], D. Schmidt[1,i], H. von der Schmitt[3], U. Schneekloth[2,e], J.A.J. Skard[6,l], J. Spitzer[3], P. Steffen[1], K. Stephens[5], A. Wagner[3], I.W. Walker[4], G. Weber[2], M. Zimmer[3,e], G.T. Zorn[6]

[1] Deutsches Elektronen-Synchrotron DESY, Hamburg, Federal Republic of Germany
[2] II. Institut für Experimentalphysik der Universität Hamburg, Hamburg, Federal Republic of Germany
[3] Physikalisches Institut der Universität Heidelberg, Heidelberg, Federal Republic of Germany
[4] University of Lancaster, Lancaster, England
[5] University of Manchester, Manchester, England
[6] University of Maryland, College Park, MD, USA
[7] Rutherford Appleton Laboratory, Chilton, Didcot, England
[8] International Center for Elementary Particle Physics, University of Tokyo, Tokyo, Japan

Received 7 August 1990

**Abstract.** The cross sections for 2-, 3- and 4-jet production have been determined with the JADE detector, sited on the $e^+e^-$-storage ring PETRA. Data at $\sqrt{s}=14$, 22, 35 and 44 GeV were compared to two $O(\alpha_s^2)$ QCD calculations. A first analysis was performed with uncorrected data using the $O(\alpha_s^2)$ 3-jet matrix element calculation of Ellis, Ross and Terrano and the Lund String Monte Carlo program. In a second analysis the calculation of Kramer and Lampe was compared to corrected data. Both approaches gave a poor description of the data when the square of the momentum transfer $Q^2=s$ was used as the scale of the running coupling constant. The description improved when the renormalization scale was adjusted to the process studied. The data were used to fix the best renormalization scale.

## 1 Introduction

The production of hadronic jets in high energy $e^+e^-$-annihilation has been studied intensively in the last few years in order to test the gauge theory of the strong interaction, Quantum Chromodynamics (QCD). Although the QCD quanta are not directly observable and thus tests of QCD predictions always depend on a hadronization model, the observation of hadronic jets is proof of the underlying parton structure. At the highest PETRA energies ($\sqrt{s}\geq 20$ GeV) jet multiplicities of 3 and more have been observed and can be explained as originating from gluon bremsstrahlung.

Up to now QCD has only been solved perturbatively. Jet cross section measurements have the attractive feature that they, to a first approximation, test different orders of the perturbative solution. For example a measurement of the 4-jet rate is essentially a test of the $O(\alpha_s^2)$ jet cross section calculations. However jet cross sections calculated in QCD are valid only for partons resolved at a given jet resolution (e.g. the minimal scaled invariant mass $y$ between any two partons) and do not take hadronization effects into account. Since the hadronization is not analytically calculable, hadronization models have to be employed to establish the relationship between the QCD jet rates and the hadron jet rates measured in the detector. Various investigations [1, 2] have shown that the 2nd order QCD calculations of the multi-jet production rates do not describe the measured data. It was

[a] Now at CERN, Geneva, Switzerland
[b] Now at MBB, Munich, FRG
[c] Now at Sheffield University, UK
[d] Now at Universität des Saarlandes, Saarbrücken, FRG
[e] Now at DESY, Hamburg, FRG
[f] Now at Bayer AG, Brunsbüttel, FRG
[g] Now at SLAC, California, USA
[h] Now at CALTECH, California, USA
[i] Universität-Gesamthochschule Wuppertal, Wuppertal, FRG
[j] Now at ESTEC, Noordwijk, Netherlands
[k] Now at University of California, Santa Cruz, California, USA
[l] Now at ST Systems Corporation, Lanham, Maryland, USA
[m] Now at Ramcke Datentechnik GmbH, Hamburg, FRG

observed that the predicted 4-jet rate is significantly lower than the measured rate. On the other hand the parton shower model JETSET [3] proved to describe the data well [4, 2]. Due to the approximations made, there is, however, no unique relationship between the $\Lambda$-parameter in the latter model and the strong coupling constant $\alpha_s$. To measure $\alpha_s$ it is therefore necessary to compare the data to complete fixed order calculations.

In perturbative QCD physical observables have only been calculated up to low orders. In addition to the uncertainties introduced due to the omission of higher order contributions this leads to a dependence of the results on the renormalization scale. The observed deficiency of the fixed order matrix elements mentioned above was found for the renormalization scale $\mu^2 = Q^2$.

In this paper the relative 2-, 3- and 4-jet production rates are compared to complete second order matrix element calculations with different renormalization scales being considered. Two analyses are presented: In the first analysis (Sect. 3) the data at 35 and 44 GeV are compared to a full Monte Carlo simulation using a matrix element based on the calculation by Ellis, Ross and Terrano (ERT) [5]. This calculation, with $E_0$ recombination scheme [6, 7] was incorporated into the JETSET 6.3 Monte Carlo program [8]. The description of the relative jet rates was optimized by varying $\Lambda_{\overline{\text{MS}}}$ and $\mu^2$ and the improvement was checked by studying various event distributions. In the second analysis (Sect. 4) the data are corrected for detector and initial state electromagnetic radiation effects. They are then compared to the calculation of Kramer and Lampe (KL') [9] modified for quark mass and hadronization effects. The renormalization scale $\mu^2$ and $\Lambda_{\overline{\text{MS}}}$ are adjusted in a simultaneous fit to the differential jet rates at all available PETRA energies, namely 14, 22, 35 and 44 GeV. The results are summarised and discussed in Sect. 5.

## 2 Renormalization scheme dependence

The definition of a renormalization scheme consists of the specification of the renormalization convention and the fixing of the renormalization scale [10], or equivalently, the fixing of the scale of the running coupling constant. In the following the $\overline{\text{MS}}$ renormalization convention [11] will be adopted. Since the scale is not a physical quantity, physical observables like cross sections do, in the limit of infinite perturbation series, not depend on the choice of the scale. In finite perturbation series, however, the scale enters as a free parameter which is not specified by the theory.

Up to $O(\alpha_s^2)$ the coupling strength at one scale $\alpha_s(\mu'^2)$ is related by the renormalization group of QCD to the coupling strength at another scale $\alpha_s(\mu^2)$ by [10, 12]

$$\alpha_s(\mu'^2) = \alpha_s(\mu^2)\left[1 - \frac{\alpha_s(\mu^2)}{2\pi} b_0 \ln\frac{\mu'^2}{\mu^2}\right] \tag{1}$$

where $b_0 = (33 - 2N_f)/6$ and $N_f$ is the number of relevant flavours.

The 2-, 3- and 4-jet cross sections are usually given by

$$\begin{aligned}
\sigma_2(y) &= 1 + A_2(y)\cdot\alpha_s(\mu^2) + B_2(y)\cdot\alpha_s^2(\mu^2)\\
\sigma_3(y) &= A_3(y)\cdot\alpha_s(\mu^2) + B_3(y)\cdot\alpha_s^2(\mu^2)\\
\sigma_4(y) &= B_4(y)\cdot\alpha_s^2(\mu^2)
\end{aligned} \tag{2}$$

where $y$ is the jet resolution parameter defined by $y = m^2/s$ with $m$ the minimum allowed invariant mass between any two partons and $s$ the square of the c.m. energy. $A_i(y)$ and $B_i(y)$ are the calculated QCD coefficients and depend only on the dimensionless cut parameter $y$. Applying (1) to incorporate the change of scale from $\mu^2$ to $\mu'^2$ one obtains expressions where the 2- and 3-jet cross section are now renormalization scale invariant up to order $\alpha_s^2$:

$$\begin{aligned}
\sigma_2(y) &= 1 + A_2(y)\cdot\alpha_s(\mu'^2)\\
&\quad + \left[B_2(y) + \frac{b_0}{2\pi}\ln\left(\frac{\mu'^2}{\mu^2}\right)A_2(y)\right]\cdot\alpha_s^2(\mu'^2)\\
\sigma_3(y) &= A_3(y)\cdot\alpha_s(\mu'^2)\\
&\quad + \left[B_3(y) + \frac{b_0}{2\pi}\ln\left(\frac{\mu'^2}{\mu^2}\right)A_3(y)\right]\cdot\alpha_s^2(\mu'^2)\\
\sigma_4(y) &= B_4(y)\cdot\alpha_s^2(\mu'^2)
\end{aligned} \tag{3}$$

A change of the scale modifies the value of $\alpha_s$ and the second order coefficients of the 2- and 3-jet cross section, since both are calculated to next-to-leading order. Due to the renormalization scale invariance these modifications cancel each other and leave the cross sections unchanged.* In contrast to these, the 4-jet cross section is only given in leading order and a change of the scale thus only affects the value of $\alpha_s$. If the 2- and 3-jet cross sections are described by the $O(\alpha_s^2)$ calculations it is thus possible to choose the scale in such a way that the calculated 2- and 3-jet cross sections are unchanged and the 4-jet cross section describes the data. Experimentally both $\Lambda_{\overline{\text{MS}}}$ and a common scale $\mu^2$ can hence be determined from a simultaneous measurement of the jet cross sections.

For the relation between $\alpha_s(\mu^2)$ and $\Lambda_{\overline{\text{MS}}}$ we adopt the convention introduced by Kramer [13]

$$\alpha_s(\mu^2) = \frac{2\pi}{b_0 \ln\dfrac{\mu^2}{\Lambda^2_{\overline{\text{MS}}}} + 2c\ln\ln\dfrac{\mu^2}{\Lambda^2_{\overline{\text{MS}}}}} \tag{4}$$

where $c = (153 - 19N_f)/(2(33 - 2N_f))$.

To overcome the scale ambiguity of the theoretical predictions in finite order several theoretical procedures have been proposed [14, 15]. A criterion establishing an appropriate choice of scale even if higher order calculations are not available has been suggested by Stevenson,

* We want to point out, that in $O(\alpha_s^2)$ due to the neglection of higher order terms, this cancellation is not perfect. In a comparison with measured data it may thus be necessary to readjust the value of $\Lambda_{\overline{\text{MS}}}$ in the definition of $\alpha_s$ if the scale $\mu^2$ is varied

the principle of minimal sensitivity (PMS) [14]. He suggests that since the full perturbation series is independent of the reference scale $\mu^2$, at fixed order the scale which minimizes the dependence on the scale is the best choice. The PMS optimization procedure can be used to fix the scale for the running coupling constant for any quantity calculated to at least next-to-leading order. Brodsky, Lepage and Mackenzie (BLM) [15] propose as a "natural" choice of scale that scale which absorbs all vacuum polarisation corrections into the coupling constant. For now the BLM scheme can only be applied to order $\alpha_s^2$ [15, 16]. In contrast to the ansatz above, where a common scale is chosen for the different cross sections, the PMS and BLM scheme yield different scales for every quantity. For the KL′ calculation of the 3-jet cross section the BLM scheme gives a scale of $\mu^2_{\mathrm{BLM}} \approx 0.1 \cdot y \cdot Q^2$ [17].

In this analysis we determine the relative 2-, 3- and 4-jet production rates and determine both $\Lambda_{\overline{\mathrm{MS}}}$ and the scale $\mu^2$ by comparison with the theoretical expressions. We investigate the scales $\mu^2 = x \cdot Q^2$ with $x$ an arbitrary number and $Q^2$ the c.m. energy squared ($Q^2 = s$). In addition we study the case $\mu^2 = y \cdot Q^2$, as proposed in early calculations of the 3-jet cross section [18–20] as a suitable scale for jet production. We compare our results for the best choice of the scale as determined by our data with both of the theoretically motivated scale choices PMS and BLM.

## 3 Comparison of theory with uncorrected data at 35 and 44 GeV

In this section the adjustment of the scale $\mu^2$ to the measured data at 35 and 44 GeV centre of mass energies is described. A detailed account of this analysis is given in [6]. To simulate measured data a Monte Carlo program was used in which the hadronization and all effects influencing the measurement such as initial state QED radiation and the limitations of the detector due to finite acceptance and resolution were taken into account. By iteratively adjusting the scale $\mu^2$ and $\Lambda_{\overline{\mathrm{MS}}}$ we determine a set of parameters that best describe the data. The results obtained from the jet cross sections were checked by studying the variation of several topological variables as a function of $\mu^2$ and $\Lambda_{\overline{\mathrm{MS}}}$.

### *3.1 Measurement of jet rates*

The data used in this part of the analysis were taken with the JADE detector at the DESY $e^+e^-$-storage ring PETRA at centre of mass energies around 35 GeV ($\int L\,dt \sim 176.0\ \mathrm{pb}^{-1}$) and 44 GeV ($\int L\,dt \sim 39.5\ \mathrm{pb}^{-1}$).

A detailed description of the JADE detector, the trigger conditions and the selection of hadronic events is given in [21].

Charged particles coming from the primary vertex with momenta above 100 MeV/$c$ and neutral particles with energies of more than 150 MeV were used. The visible energy in the event, $E_{\mathrm{vis}}$, was calculated assuming that charged particles be pions and neutral particles be photons. In order to select clean multihadronic events one additional cut was applied. For each event the missing momentum had to be smaller than 30% of $\sqrt{s}$. The event sample then consists of 36159 events at 35 GeV and 4747 events at 44 GeV. The background was found to be less than 1% from $\tau$-pair events and less than 0.1% from 2-$\gamma$ events and can safely be neglected for this investigation.

A jet reconstruction algorithm based on the algorithm YCLUS [1, 22] was used to determine the jet cross sections in the data and in the Monte Carlo events. This algorithm follows approximately the definition of the ERT $E_0$ prescription for resolved partons [6, 7] and works as follows: In each hadronic event the quantities

$$y_{kl} = \frac{2 E_k E_l (1 - \cos\theta_{kl})}{E^2_{\mathrm{vis}}} \tag{5}$$

are calculated for all pairs of particles $k$ and $l$, assuming in the first step these to be massless. If the smallest $y_{kl}$ is less than a prescribed threshold value $y_{\mathrm{cut}}$ the two particles $k$ and $l$ are replaced by a pseudoparticle or "cluster" with the four-momentum $(p_k + p_l)$. This procedure is repeated until all combinations $y_{kl}$ exceed the threshold value $y_{\mathrm{cut}}$. The clusters are then considered to be "jets". It should be emphasized that measured physical quantities may not depend on details of the jet reconstruction algorithm. The reconstruction algorithm applied in the second analysis (Sect. 4) is also based on YCLUS, but the definition differs from the above in that in the first step charged particles $k$ and $l$ in (5) are assumed to be pions.

In Fig. 1 the measured jet rates $\sigma_{n-\mathrm{jet}}(y_{\mathrm{cut}})/\sigma_{\mathrm{tot}}$, ($n = 2, 3, 4$), where $\sigma_{\mathrm{tot}}$ is the total hadronic cross section and $\sigma_{n-\mathrm{jet}}(y_{\mathrm{cut}})$ the $n$-jet production cross section, as a function of the threshold value $y_{\mathrm{cut}}$, are compared to the rates in the Monte Carlo event samples with $\mu^2 = Q^2$ for the scale of the running coupling constant. Although we used a slightly different definition of the jet reconstruction algorithm the measured rates in the data agree well with the results of a previous analysis [23]. The measured 5-jet rate for $y_{\mathrm{cut}} \geqq 0.02$ is less than 1% and was ignored in this analysis. In the Monte Carlo event samples three different values of $\Lambda_{\overline{\mathrm{MS}}}$ have been used. In the range $\Lambda_{\overline{\mathrm{MS}}} = [200\text{–}300]$ MeV the ERT $E_0$ matrix element gives a good description of the 2- and 3-jet rate but fails to describe the 4-jet rate. The range was estimated from Monte Carlo samples where different values for $\Lambda_{\overline{\mathrm{MS}}}$ were used.

The 4-jet rate predicted by the $O(\alpha_s^2)$ theory is about 50% of the measured rate at both energies. Comparison of the jet rates in the data with the $O(\alpha_s^2)$ calculation of GKS in earlier JADE studies [1, 22, 24] and by the MARK-II [4] and TASSO collaboration [2] yielded similar results.

*3.1.1 Changing the renormalization scale.* In the second step of the analysis the scale $\mu^2$ in the Monte Carlo generator was changed to the PMS scales of the 2-jet

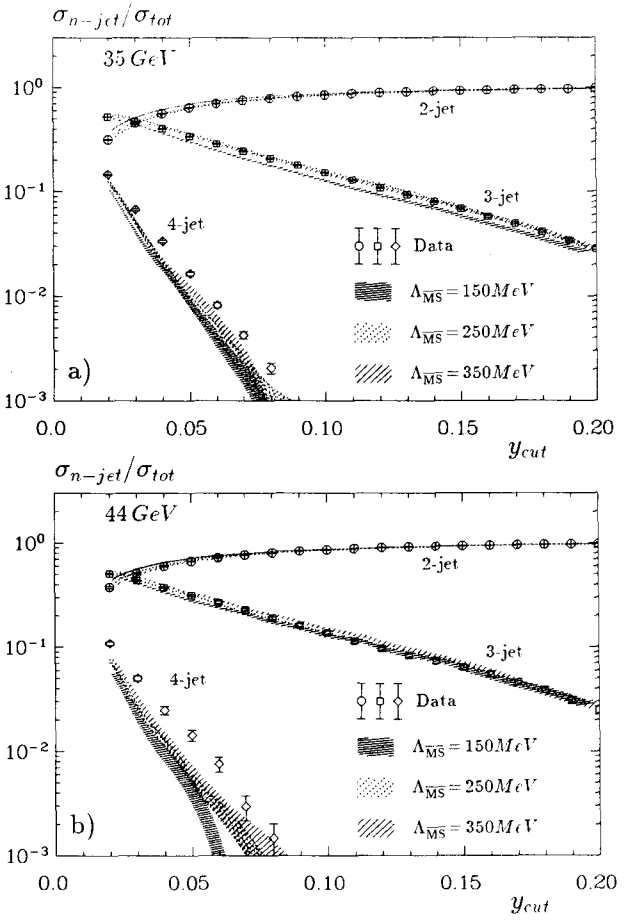


**Fig. 1a, b.** Comparison of the measured jet rates at **a** 35 GeV and **b** 44 GeV to the Monte Carlo jet rates for $\mu^2 = Q^2$ and different values of $\Lambda_{\overline{MS}}$. The statistical error in the Monte Carlo simulation corresponds to the width of the bands

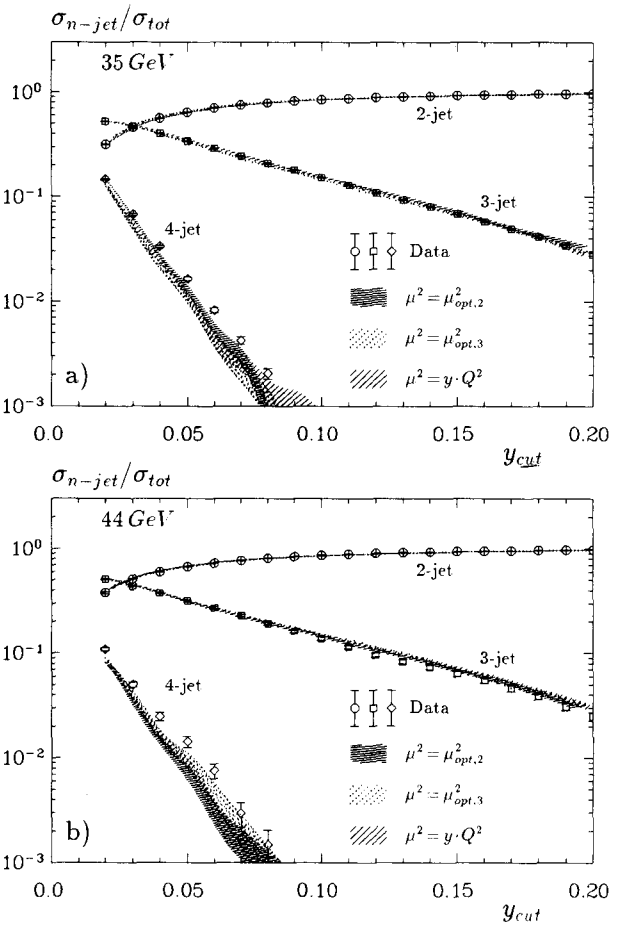


**Fig. 2a, b.** Comparison of the measured jet rates at **a** 35 GeV and **b** 44 GeV to the Monte Carlo jet rates with the PMS scales $\mu^2_{opt,2}$ and $\mu^2_{opt,3}$ and the scale $y \cdot Q^2$ for $\Lambda_{\overline{MS}} = 90$, 120 and 90 MeV, respectively. The statistical error in the Monte Carlo simulation corresponds to the width of the bands

cross section in the KL′ calculation $\mu^2_{opt,2}$ and of the ERT $E_0$ 3-jet cross section $\mu^2_{opt,3}$. It was impossible to determine the optimized scale for the 4-jet cross section as the PMS optimization for this observable requires an $O(\alpha_s^3)$calculation. Since this was not available we assumed that the optimized scales derived from the 2- and 3-jet cross sections apply also to the 4-jet cross section. These scales and also the scale $y \cdot Q^2$ were used in the Monte Carlo program to generate events. The factor $y$ used in the Monte Carlo generator is set to be cut-off $y_{min} (= 0.015)$ in the parton generator. This is different from the minimum $y$ in the individual event. Due to the smallness of the involved $y$ values the influence of this difference was estimated to be small.

This change of the scale for the running coupling constant $\alpha_s(\mu^2)$ resulted in a better agreement between the 4-jet rate in the data and in the Monte Carlo simulation leaving the 2- and 3-jet rates unchanged, as shown in Fig. 2. In order to achieve this improved agreement it is necessary to decrease $\Lambda_{\overline{MS}}$ from 250 MeV (with the scale $\mu^2 = Q^2$) to 90 MeV (with the scales $\mu^2 = \mu^2_{opt,2}$ and $\mu^2 = y \cdot Q^2$) or to 120 MeV (with the scale $\mu^2 = \mu^2_{opt,3}$). This is in agreement with the renormalization scale invariance of the 2- and 3-jet cross sections as given by (3) but the dependence of $\Lambda_{\overline{MS}}$ on the scale shows that the neglected higher order terms in the perturbation expansion are significant.

A further ansatz that may be used to choose an optimal scale is to look for that scale which, when used in QCD calculations to the order available, gives the best agreement with the data. Applying this principle here in the third step of the analysis, the scale of the running coupling constant was iteratively adjusted so that the jet rates in the data were described by the $O(\alpha_s^2)$ ERT matrix element. It was found that the scale of the running coupling constant had to be decreased to $0.005 \cdot Q^2$ in order to give a satisfactory description of the measured 4-jet rate. In Fig. 3 the jet rates in the data are compared with the Monte Carlo simulation using the best values for $\Lambda_{\overline{MS}}$. Note that although in Fig. 3 an even smaller scale $\mu^2 = 0.001 \cdot Q^2$ gives a better description of the 4-jet rate the resulting description of the 3-jet rate is poor.

In agreement with the conjecture of the PMS optimization procedure which gives for $y > 0.02$ scales close to $0.005 \cdot Q^2$, $\Lambda_{\overline{MS}}$ did not have to be changed here. The

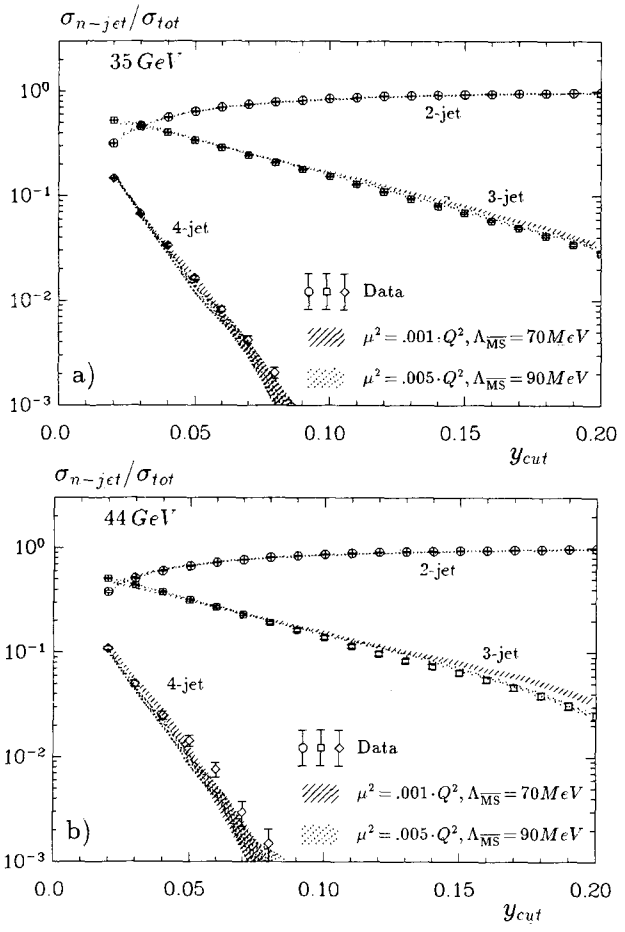


**Fig. 3a, b.** Comparison of the measured jet rates at **a** 35 GeV and **b** 44 GeV to the Monte Carlo jet rates with different choices for the scale and $\Lambda_{\overline{MS}}$. The statistical error in the Monte Carlo simulation corresponds to the width of the bands

iterative procedure of testing many different combinations of scales and values for $\Lambda_{\overline{MS}}$ in the Monte Carlo generator resulted in ranges for $\mu^2$ and $\Lambda_{\overline{MS}}$ that are compatible with the measured data of $\mu^2 = [0.003\text{–}0.007] \cdot Q^2$ and $\Lambda_{\overline{MS}} = [50\text{–}130]$ MeV. The best description of the data was found for the scale $\mu^2$ of $0.005 \cdot Q^2$ and a value for $\Lambda_{\overline{MS}}$ of 90 MeV.

*3.1.2 Event structure.* In addition to the missing 4-jet fraction previous analyses [1, 22, 24] showed that some event topology distributions are poorly described by the $O(\alpha_s^2)$ Monte Carlo simulation in which the scale $Q^2$ is used in the running coupling constant. To check the influence of the scale changes on the event topology, acoplanarity $A$ [25], aplanarity $AP = \frac{3}{2} Q_1$, thrust $T$ [26, 27] and sphericity $S = \frac{3}{2}(Q_1 + Q_2)$ [28] distributions were studied. Here $Q_1 < Q_2 < Q_3$ (with $Q_1 + Q_2 + Q_3 = 1$) are the normalized ordered eigenvalues of the momentum tensor $M_{\alpha\beta} = \sum_j p_{\alpha j} p_{\beta j}$, where $\alpha$ and $\beta$ refer to the $x$, $y$ and $z$ components and the sum extends over all particles in the event. The eigenvector $\mathbf{n}_3$ defines the sphericity axis and $\mathbf{n}_3$ and $\mathbf{n}_2$ define the event plane. The distribution of $p_T^{out}$, the momentum perpendicular to the event plane, was studied as an example of a single particle distribution.

We confirmed that $A$ and $AP$ are badly described when the scale $Q^2$ is used in the running coupling constant. The $\chi^2$ values for the comparison between the experimental distributions and the Monte Carlo simulation are listed in Table 1. When the scale is changed to $y \cdot Q^2$ or to the PMS scales the agreement between data and Monte Carlo for the event topology distributions improves. The corresponding values for the sum of $\chi^2$ per degree of freedom for the different scales and the investigated topological variables are also shown in Table 1. It was observed that the values for the scale and $\Lambda_{\overline{MS}}$ which gave the best description of the jet rates also best describe the topological variables studied. This was expected since most of the distributions studied are highly correlated to the number of jets in the event. Whereas $S$ and $T$ are mainly dependent on the number of 2-jets and 3-jets, respectively, and thus depend only weakly on the scale, $A$, $AP$ and $p_T^{out}$ depend strongly on the number of multijets. This is confirmed by the dependence of the quality of the fit for $A$ and $AP$ on $\mu^2$. That the description of the $p_T^{out}$ distribution does not improve for

**Table 1.** Quality of the fits of the $A$, $AP$, $T$, $S$ and $p_T^{out}$ distributions at $\sqrt{s} = 35$ and 44 GeV using the ERT $E_0$ matrix element in the JETSET 6.3 Monte Carlo at the listed renormalization scales and values for $\Lambda_{\overline{MS}}$

| Variable | $\mu^2 = Q^2$ $\Lambda_{\overline{MS}} = 250$ MeV | $\mu^2 = y \cdot Q^2$ $\Lambda_{\overline{MS}} = 90$ MeV | $\mu^2 = \mu^2_{opt,2}$ $\Lambda_{\overline{MS}} = 90$ MeV | $\mu^2 = \mu^2_{opt,3}$ $\Lambda_{\overline{MS}} = 120$ MeV | $\mu^2 = 0.005 \cdot Q^2$ $\Lambda_{\overline{MS}} = 90$ MeV |
|---|---|---|---|---|---|
| | $\chi^2$/d.o.f. at $\sqrt{s} = 35$ GeV | | | | |
| $A$ | 147.0/24 | 108.1/24 | 88.9/24 | 126.8/24 | 39.6/24 |
| $AP$ | 127.2/29 | 106.5/29 | 87.6/29 | 123.4/29 | 34.9/29 |
| $T$ | 26.3/21 | 33.1/21 | 28.1/21 | 49.1/22 | 9.1/21 |
| $S$ | 130.9/79 | 137.9/79 | 84.3/79 | 122.9/78 | 121.1/78 |
| $p_T^{out}$ | 406.4/46 | 380.0/46 | 375.8/47 | 388.6/46 | 237.2/46 |
| | $\chi^2$/d.o.f. at $\sqrt{s} = 44$ GeV | | | | |
| $A$ | 135.1/24 | 45.0/24 | 52.7/24 | 74.6/24 | 29.5/23 |
| $AP$ | 106.3/27 | 30.1/24 | 35.1/24 | 55.7/24 | 25.0/25 |
| $T$ | 40.7/21 | 30.4/21 | 23.4/20 | 38.3/20 | 12.2/21 |
| $S$ | 84.8/75 | 78.8/76 | 87.7/76 | 96.9/76 | 82.1/76 |
| $p_T^{out}$ | 418.6/46 | 317.1/45 | 367.5/45 | 431.8/45 | 329.8/45 |

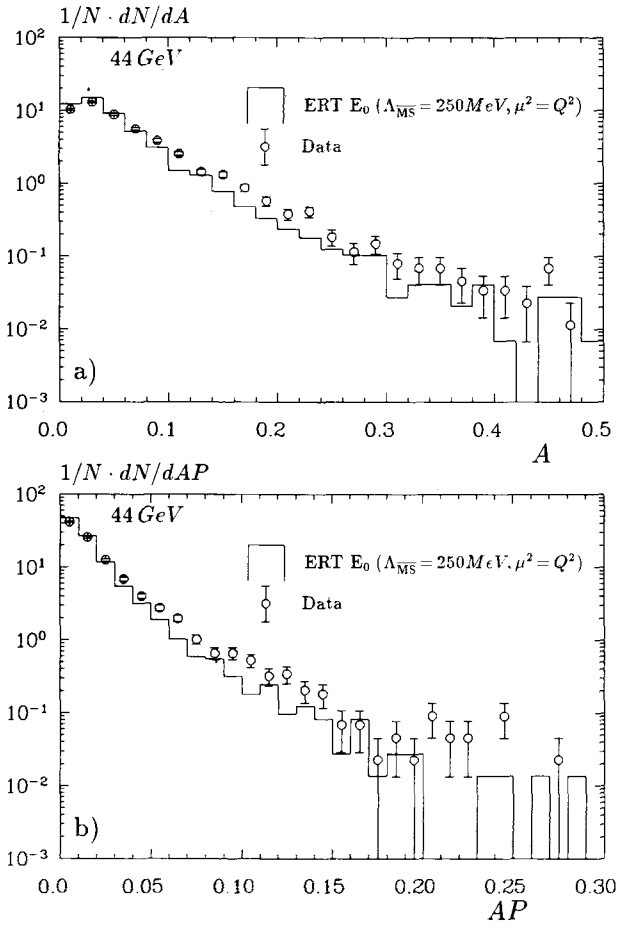


**Fig. 4a, b.** Acoplanarity $A$ **a** and Aplanarity $AP$ **b** in the 44 GeV data and the ERT $E_0$ Monte Carlo events for the scale $Q^2$ and $\Lambda_{\overline{\text{MS}}}=250$ MeV

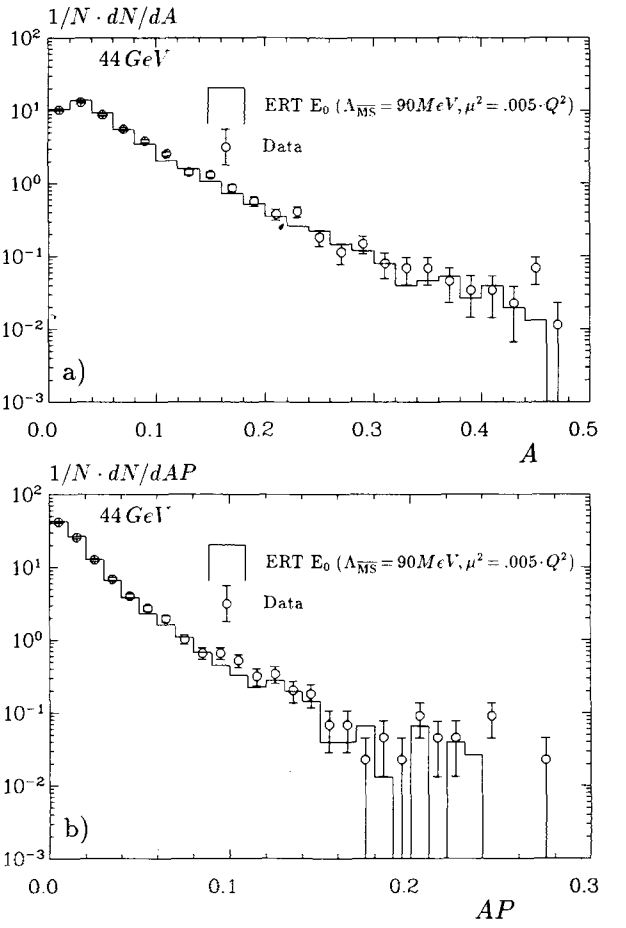


**Fig. 5a, b.** Acoplanarity $A$ **a** and aplanarity $AP$ **b** in the 44 GeV data and the ERT $E_0$ Monte Carlo for the scale $\mu^2=0.005\cdot Q^2$ and $\Lambda_{\overline{\text{MS}}}=90$ MeV

smaller scales $\mu^2$ is an indicative of additional hadronization effects not taken into account or not yet understood.

The $A$ and $AP$ distributions of the 44 GeV data and Monte Carlo simulation for the scale $Q^2$ and $\Lambda_{\overline{\text{MS}}}=250$ MeV is shown in Fig.4. The same distributions for the scale $0.005\cdot Q^2$ and $\Lambda_{\overline{\text{MS}}}=90$ MeV is shown in Fig. 5. As shown in Table 1 the description of the $p_T^{\text{out}}$ distributions is only slightly improved. In Fig. 6 the $p_T^{\text{out}}$ distributions of the 44 GeV data and the Monte Carlo simulation are shown for the scale $Q^2$ and $\Lambda_{\overline{\text{MS}}}=250$ MeV (a) and for the scale $0.005\cdot Q^2$ and $\Lambda_{\overline{\text{MS}}}=90$ MeV (b).

## 4 Comparison of theory with corrected data at 14, 22, 35 and 44 GeV

In this section we describe a simultaneous fit of $\Lambda_{\overline{\text{MS}}}$ and the scale $\mu^2$ to the data at all available energies. A detailed account of the analysis is given in [29]. We used the following procedure. In a first step the data were corrected for effects of the detector resolution, selection criteria and initial state radiation. The QCD expectations [9] which depend on $\mu^2$ and $\Lambda_{\overline{\text{MS}}}$ were modified to take into account the effects of hadronization and of finite quark masses. The expressions thus obtained were then compared with the data and $\mu^2$ and $\Lambda_{\overline{\text{MS}}}$ extracted from a simultaneous fit to the corrected data.

### *4.1 Correction of the experimental jet rates for detector and initial state radiation effects*

The data considered were taken at four centre of mass energies between 14 and 44 GeV. Both neutral and charged particles were used in the analysis. The selection criteria deviated from those used in Sect. 3 in the additional requirements:

- visible energy $E_{\text{vis}}$: $0.5\sqrt{s}\leqq E_{\text{vis}}\leqq\sqrt{s}$
- missing momentum $p_{\text{miss}}=|\sum_i \mathbf{p}^i|<0.25\sqrt{s}$

The numbers of events satisfying these criteria are given in Table 2.

The experimental 2-, 3-, 4- and 5-jet rates ($R_i$, $i=2$–5) as a function of the resolution parameter $y_{\text{cut}}$ were obtained with the cluster algorithm described in Sect. 3. Since the jet rate does not depend on a particular bin size definition, we chose in all calculations of the follow-

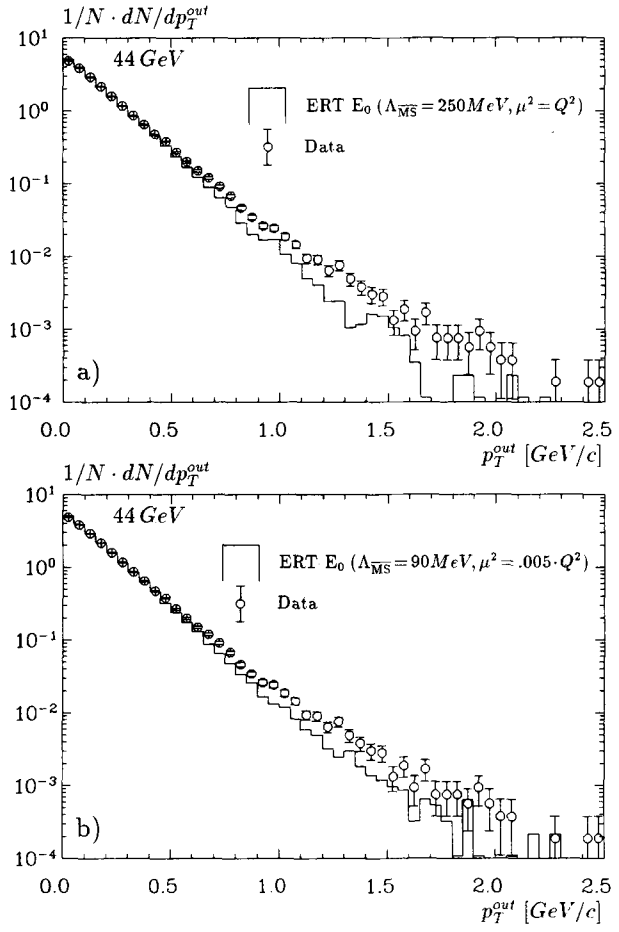


**Fig. 6a, b.** $p_T^{out}$ distribution in the 44 GeV data and in the ERT $E_0$ Monte Carlo for the scale $Q^2$ and $\Lambda_{\overline{MS}} = 250$ MeV **a** and for the scale $\mu^2 = 0.005 \cdot Q^2$ and $\Lambda_{\overline{MS}} = 90$ MeV **b**

**Table 2.** The samples of selected multihadronic events

| $\sqrt{s}$ [GeV] | Number of events | $\int L dt$ |
|---|---|---|
| 14 | 1699 | 1.6 pb$^{-1}$ |
| 22 | 1130 | 2.7 pb$^{-1}$ |
| 35 | 25829 | 176 pb$^{-1}$ |
| 44 | 3312 | 39.5 pb$^{-1}$ |

ing analysis a small bin width of 0.001. In order to avoid counting isolated high energy photons as jets, a minimum of two particles was required to define a jet i.e. $N_{\text{particles}} \geqq 2$. Because of this cut a 1-jet rate of the order 0.05% was obtained. This was ignored in the following analysis.

The unfolding of detector resolution and acceptance as well as initial state radiation was done with the parton shower version of the Lund hadronization model JETSET 6.3. This model describes the data at all centre of mass energies well [1, 29] with one set of parameters*.

* $A = 0.5$, $B = 0.9$ GeV$^{-2}$, $\varepsilon_c = 0.05$, $\varepsilon_b = 0.01$, $\sqrt{2} \cdot \sigma_q = 425$ MeV, $Q_0 = 1$ GeV/c$^2$, $\Lambda_{LLA} = 400$ MeV

For the correction two Monte Carlo samples were generated.

(1) The first one was for a perfect detector with infinite resolution and no initial state radiation applied. All particles with a lifetime larger than $10^{-10}$ sec – i.e. particles with a lifetime larger than $K_S^0$ – were treated as stable. The jet rates were then computed from the charged and neutral final state particles including $K_L^0$'s, neutrons and neutrinos and denoted here by $R_{MC}^{\text{no detector}}(y_{cut})$. (2) For the second sample a full simulation of the JADE detector was carried out and initial state radiation was applied. Particles with lifetimes such that they would decay in the sensitive part of the detector were allowed to decay. All effects of resolution, acceptance and selection were taken into account. The jet rates were computed from the reconstructed charged and neutral particles and denoted here by $R_{MC}^{\text{detector}}(y_{cut})$.

For each bin in $y_{cut}$ a correction factor $C(y_{cut}) = R_{MC}^{\text{no detector}}(y_{cut})/R_{MC}^{\text{detector}}(y_{cut})$ was calculated. The corrected integrated jet rates $R_i$ ($i = 2$–5) where then obtained by multiplying the uncorrected data with this correction factor bin by bin. For the range $0.02 < y_{cut} < 0.14$ (the range used later for the fit) the correction factors are close to unity and typically do not deviate by more than 10% from unity for energies larger then 14 GeV. At 14 GeV, where quark mass effects are substantial, the correction factors for $R_4$ and $R_5$ are larger and approach the value of 1.5 at some values of $y_{cut}$.

The unfolded jet rates are shown in Fig. 7 as a function of $y_{cut}$ and with a bin size of 0.01.

### *4.2 Correction of theoretical jet rates due to mass and hadronization effects*

The QCD jet rate calculation of Kramer and Lampe, (2), cannot be directly compared with the corrected jet rates for two reasons:

(a) QCD calculations for massive partons exist only to first order in $\alpha_s$ [30, 31]. The full second order expressions are valid only for massless partons. The effects of finite masses have to be studied and taken into account where necessary.

(b) The QCD expressions are rates of partons, whereas the corrected data are rates of jets. Corrections for hadronization have to be applied.

We chose to apply both corrections to the theoretical expressions.

*Mass correction.* This correction was applied bin by bin as in the case of the detector correction described in Sect. 4.1. It was obtained from the JETSET 6.3 hadronization model with ERT $E_0$ matrix element [7] for fixed values of $\Lambda_{\overline{MS}}$ and scale $\mu^2$. The dependence of the mass correction on $\Lambda_{\overline{MS}}$ and $\mu^2$ is small and was neglected. In that model the number of kinematical configurations of massless partons is generated in accordance with the $O(\alpha_s^2)$ matrix element. The kinematic effect of massive quarks are taken into account by assigning finite masses to the partons and then rescaling the momenta to ensure

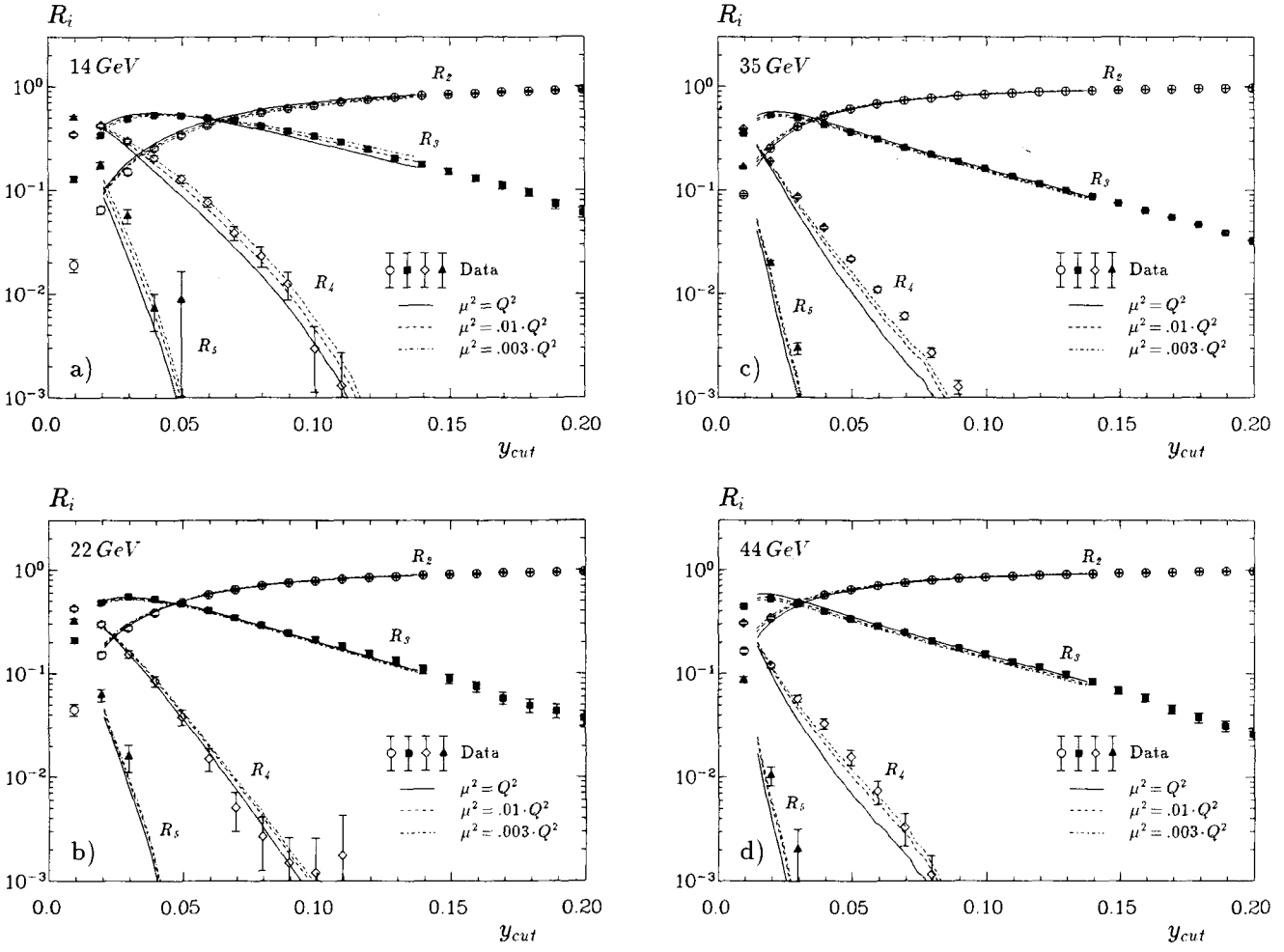


**Fig. 7a–d.** Unfolded jet rates as a function of $y_{cut}$ at **a** 14 GeV, **b** 22 GeV, **c** 35 GeV and **d** 44 GeV compared with the results from the simultaneous fit (the explanation is given in Sect. 4.4)

energy conservation. The resulting changes in the parton rates were investigated by calculating the relative rates as a function of $y$ for the case of $u$-quarks alone ($R^u_{i\,\text{partons}}(y)$) and for the correct mixture of quarks ($R^{udscb}_{i\,\text{partons}}(y)$). The correction factor $k_i$ with which the theoretical parton rates have to be multiplied is then just the ratio $k_i(y) = R^{udscb}_{i\,\text{partons}}(y)/R^u_{i\,\text{partons}}(y)$. At $y = 0.08$ the correction factor varies from about 0.92 at $\sqrt{s} = 14$ GeV to 0.99 at $\sqrt{s} = 44$ GeV*. The resultant change of the 4-parton rate is small and was neglected in the analysis. Thus only the 3-parton rate was corrected by $k_3(y)$ and the 2-parton rate recalculated from the sum rule $R_{2\,\text{partons}} = 1 - k_3 R_{3\,\text{partons}} - R_{4\,\text{partons}}$.

Note that this method of obtaining the mass correction only takes into account the kinematical effects of the quark masses. In the absence of dynamical QCD calculations for massive quarks to second order in $\alpha_s$ it is impossible to do better than this. We make allowance for this uncertainty in the systematic error.

* The correction factor for the 3-parton rate can be linearly parametrized as a function of $y$: $k_3(y) = a \cdot y + b$

*Correction for hadronization.* The correction of the analytical $O(\alpha_s^2)$ calculation for the effects of hadronization and the cluster algorithm can formally be written as

$$R_j^{\text{corr}}(y_{\text{cut}}) = \sum_{i=2}^{4} \sum_{k=2}^{i} P_k^i(y = y_{\text{cut}})\, M_{kj}^i(y_{\text{cut}}); \quad j = 2\text{–}5, \qquad (6)$$

where $R_j^{\text{corr}}(y_{\text{cut}})$ is the theoretical relative jet rate in $O(\alpha_s^2)$, corrected for the effects of hadronization. The theoretical 5-jet rate enters here only as a consequence of hadronization effects. The coefficient $P_k^i(y)$ is the proportion of $i$-parton events, at a resolution of $y_{\text{min}}$, which are resolved as containing $k$ partons, at a resolution of $y$. The $M_{kj}^i(y_{\text{cut}})$ are the probabilities that a given event is reconstructed as a $j$-jet event after hadronization, for the case that it had $i$ partons at $y = y_{\text{min}}$ and $k$ partons resolved at $y \geqq y_{\text{min}}$. The probabilities $M_{kj}^i(y_{\text{cut}})$ are calculated from Monte Carlo simulation using the ERT $E_0$ matrix element as a function of $y_{\text{cut}}$ and the centre of mass energy. An ideal detector without simulation of initial state radiation could be used since these effects were unfolded from the data. The hadronization parame-

**Table 3.** Model parameters

| $\sqrt{s}$ [GeV] | 14 | 22 | 35 | 44 |
|---|---|---|---|---|
| $A$ | 0.4 | 0.7 | 1.0 | 1.0 |
| $B$ [GeV$^{-2}$] | 0.6 | 0.6 | 0.6 | 0.6 |
| $\varepsilon_c$ | 0.015 | 0.025 | 0.05 | 0.05 |
| $\varepsilon_b$ | 0.002 | 0.007 | 0.018 | 0.018 |
| $y_{\min}$ | 0.02 | 0.02 | 0.015 | 0.015 |
| $\Lambda_{\overline{\text{MS}}}$ [MeV] | 250 | 250 | 250 | 250 |

ters in the model were varied with $\sqrt{s}$ such that the model describes the data at all energies [32–34]. Table 3 lists the parameter values used. The $P_k^i(y)$ can be written as follows:

$$P_2^2(y)=\sigma_0/\sigma_{\text{tot}}\cdot\{1+\alpha_s A_2(y_{\min})+\alpha_s^2 B_2(y_{\min})\}$$

$$P_2^3(y)=\sigma_0/\sigma_{\text{tot}}\cdot\{\alpha_s[A_2(y)-A_2(y_{\min})]+\alpha_s^2[B_2(y)-B_2(y_{\min})-B_2^{\text{soft}\,4}(y)]\}$$

$$P_2^4(y)=\sigma_0/\sigma_{\text{tot}}\cdot\{\alpha_s^2 B_2^{\text{soft}\,4}(y)\}$$

$$P_3^3(y)=\sigma_0/\sigma_{\text{tot}}\cdot\{\alpha_s A_3(y)+\alpha_s^2[B_3(y)-B_3^{\text{soft}\,4}(y)]\}$$

$$P_3^4(y)=\sigma_0/\sigma_{\text{tot}}\cdot\{\alpha_s^2 B_3^{\text{soft}\,4}(y)\}$$

$$P_4^4(y)=\sigma_0/\sigma_{\text{tot}}\cdot\{\alpha_s^2 B_4(y)\} \qquad (7)$$

Here $\sigma_0$ is the electromagnetic Born cross section for the production of 5 quark flavours and $\sigma_{\text{tot}}$ the total hadronic cross section. The $A_i$ and $B_i$ are the QCD coefficients of (3) numerically calculated in [9]. The $B_i^{\text{soft}\,4}(y)$ is the contribution of configurations with originally 4 partons at $y=y_{\min}$ giving $i$ partons, ($i=2, 3$) resolved at $y$ and was also determined by Monte Carlo. As a cross check it can easily be deduced from (7) that the sum $P_2^2(y)+P_2^3(y)+P_2^4(y)$ is equal to the right hand side of (2) up to the factor $\sigma_0/\sigma_{\text{tot}}$, as has to be the case for the total total fraction of 2-parton events at $y$. The same is true for the total 3- and 4-parton classes.

The effect of the hadronization correction is illustrated in Fig. 8. It shows the Monte Carlo parton rates, both uncorrected and corrected, for the two centre of mass energies 14 and 44 GeV. Whereas the correction is substantial at the lower energy it is almost negligible at high energies. At 22 and 35 GeV the corrections lie between those shown in Fig. 8a) and b). With the parton classes $P_k^i(y)$ split up as defined in (7), the jet reconstruction probabilities $M_{kj}^i(y_{\text{cut}})$ in (6) turn out to be essentially independent of the value of $\alpha_s$ (or $\Lambda_{\overline{\text{MS}}}$ and $\mu^2$) used in the simulation*. This is important for the following fit of the scale $\mu^2$ and $\Lambda_{\overline{\text{MS}}}$ since a change of the scale involves, as discussed in Sect. 2, a change of the coupling strength.

* Had we adopted the simpler correction procedure $R_j^{\text{corr}}(y_{\text{cut}})=\sum_{i=2}^{4} P^i(y=y_{\text{cut}})M_j^i(y_{\text{cut}})$ the matrix $M_j^i$ would have been strongly dependent on $\alpha_s$

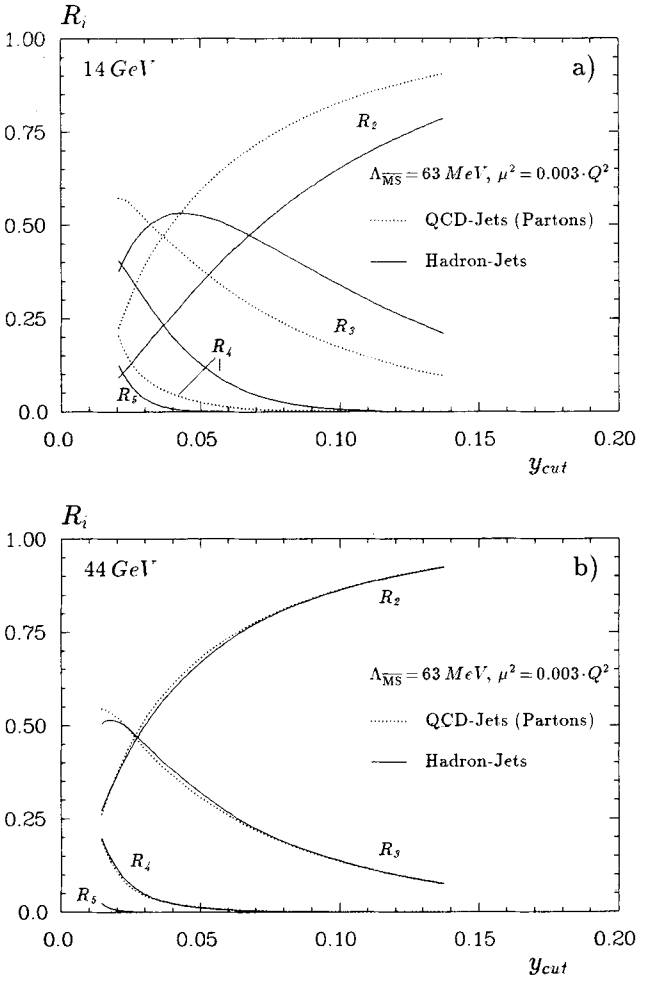


**Fig. 8a, b.** Comparison of the theoretical jet rates before (resolved partons) and after hadronization (hadrons) for **a** 14 GeV and **b** 44 GeV

### *4.3 Differential jet rates*

Using the results of Sect. 4.2 the experimental jet rates (Fig. 7) can be directly compared with the modified theoretical expressions (6). In doing so, one has to consider, that the data points in Fig. 7 are highly correlated in several ways: Since the jet rates are integrated from zero up to $y_{\text{cut}}$, an event which enters the distribution for $i$ jets at a particular $y$ and leaves it at, say, $y'$ contributes at all points between $y$ and $y'$. A second correlation comes from the sum rule obeyed by the jet rates $\sum_{j=2}^{5} R_j = 1$. Both correlations can largely be avoided if one constructs three new distributions defined as follows:

$$D_2(y_{\text{cut}})=N\cdot[R_2(y_{\text{cut}}+\Delta y)-R_2(y_{\text{cut}})]$$

$$D_3(y_{\text{cut}})=N\cdot[R_3(y_{\text{cut}}+\Delta y)-R_3(y_{\text{cut}})]+D_2(y_{\text{cut}})$$

$$D_4(y_{\text{cut}})=N\cdot[R_4(y_{\text{cut}}+\Delta y)-R_4(y_{\text{cut}})]+D_3(y_{\text{cut}}), \qquad (8)$$

where $N$ is the number of events observed at a given centre of mass energy (Table 2), and $\Delta y$ is the bin width

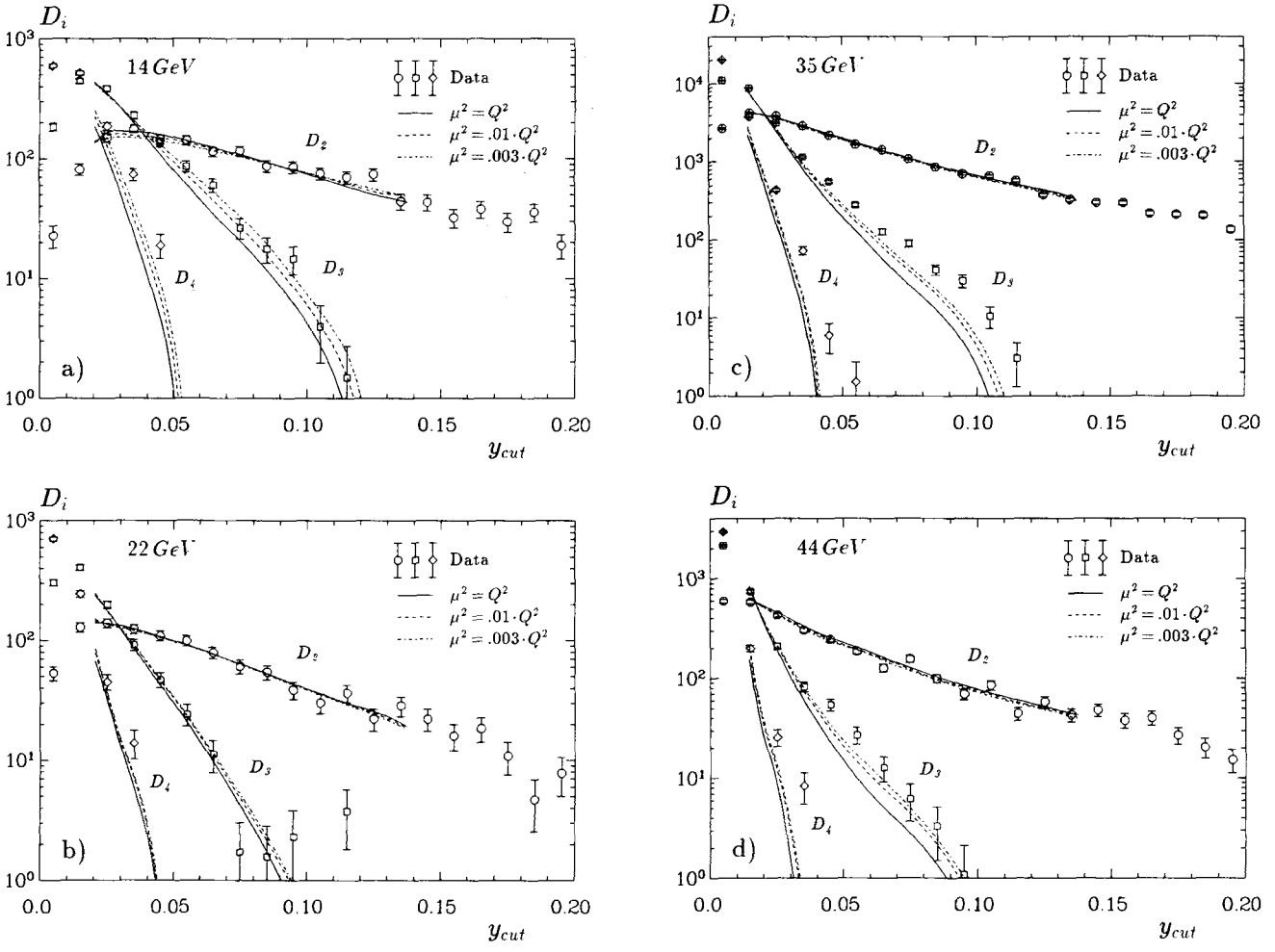


**Fig. 9a–d.** Differential distributions as a function of $y_{cut}$ at **a** 14 GeV **b** 22 GeV **c** 35 GeV and **d** 44 GeV. The curves present the simultaneous fit to all $D_i$-distributions for different parametrization of the scale $\mu^2$

**Table 4.** The total number of events in the $D$-distributions as a function of $y_{cut}$ and with the bin width $\Delta y_{cut} = 0.01$. The statistical errors are given by $\sqrt{D_i}$

| $y_{cut}$ | $\sqrt{s}=14$ GeV | | | $\sqrt{s}=22$ GeV | | | $\sqrt{s}=35$ GeV | | | $\sqrt{s}=44$ GeV | | |
|---|---|---|---|---|---|---|---|---|---|---|---|---|
| | $D_2$ | $D_3$ | $D_4$ | $D_2$ | $D_3$ | $D_4$ | $D_2$ | $D_3$ | $D_4$ | $D_2$ | $D_3$ | $D_4$ |
| 0.005 | 23 | 183 | 592 | 53 | 305 | 706 | 2694 | 12341 | 21180 | 593 | 2136 | 293 |
| 0.015 | 81 | 444 | 515 | 128 | 407 | 245 | 4260 | 8151 | 3023 | 584 | 747 | 200 |
| 0.025 | 149 | 384 | 186 | 140 | 199 | 45 | 3846 | 2814 | 367 | 431 | 209 | 26 |
| 0.035 | 176 | 228 | 73 | 124 | 92 | 14 | 2892 | 1068 | 60 | 303 | 83 | 8 |
| 0.045 | 145 | 136 | 19 | 109 | 47 | – | 2193 | 537 | 2 | 247 | 55 | – |
| 0.055 | 142 | 86 | – | 99 | 24 | – | 1685 | 264 | 3 | 189 | 27 | – |
| 0.065 | 114 | 60 | – | 79 | 11 | – | 1428 | 114 | – | 127 | 13 | – |
| 0.075 | 115 | 26 | – | 61 | 2 | – | 1082 | 83 | – | 156 | 6 | – |
| 0.085 | 86 | 18 | – | 54 | 2 | – | 851 | 34 | – | 99 | 3 | – |
| 0.095 | 84 | 15 | – | 39 | 2 | – | 694 | 15 | – | 69 | 1 | – |
| 0.105 | 75 | 4 | – | 30 | 1 | – | 652 | 23 | – | 85 | – | – |
| 0.115 | 70 | 1 | – | 36 | 4 | – | 571 | 7 | – | 44 | – | – |
| 0.125 | 73 | – | – | 22 | – | – | 373 | – | – | 58 | – | – |
| 0.135 | 44 | – | – | 29 | – | – | 324 | – | – | 43 | – | – |
| 0.145 | 43 | – | – | 22 | – | – | 299 | – | – | 48 | – | – |
| 0.155 | 32 | – | – | 16 | – | – | 297 | – | – | 38 | – | – |
| 0.165 | 38 | – | – | 18 | – | – | 217 | – | – | 40 | – | – |
| 0.175 | 30 | – | – | 11 | – | – | 212 | – | – | 27 | – | – |
| 0.185 | 35 | – | – | 5 | – | – | 205 | – | – | 20 | – | – |
| 0.195 | 19 | – | – | 8 | – | – | 135 | – | – | 15 | – | – |

**Table 5.** The unfolded 2-, 3-, and 4-jet rates for $y_{cut}=0.005$. The 5-jet rate can be calculated from the sum rule $R_5=1-R_2-R_3-R_4$

| $\sqrt{s}$ | $R_2(y_{cut}=0.005)$ | $R_3(y_{cut}=0.005)$ | $R_4(y_{cut}=0.005)$ |
|---|---|---|---|
| 14 GeV | 0.013350 | 0.068184 | 0.22344 |
| 22 GeV | 0.015134 | 0.090556 | 0.26979 |
| 35 GeV | 0.030216 | 0.168360 | 0.36690 |
| 44 GeV | 0.065480 | 0.277780 | 0.38135 |

**Table 6.** $\Lambda_{\overline{MS}}$ values obtained from the fit of the theory of $D_2(y_{cut})$, $D_3(y_{cut})$ and $D_4(y_{cut})$ at all energies. The errors are the statistical errors of the fit

| Skala $\mu^2$ [(GeV)$^2$] | $\Lambda_{\overline{MS}}$ [MeV] | $\chi^2$/d.o.f. |
|---|---|---|
| $1\cdot Q^2$ | $269\pm7.2$ | 1.92 |
| $0.1\cdot Q^2$ | $143\pm4.2$ | 1.69 |
| $0.01\cdot Q^2$ | $83\pm1.9$ | 1.41 |
| $0.003\cdot Q^2$ | $63\pm1.5$ | 1.28 |
| $y\cdot Q^2$ | $96\pm2.8$ | 1.64 |
| $\mu^2_{opt,2}(y)$, $\mu^2_{opt,3}(y)$ | $83\pm2.3$ | 1.48 |

used. It can be verified that the $D_i$ are not correlated through a sum rule and that each event enters each $D$-distribution (i.e. $D_2$, $D_3$ and $D_4$) only once. The $D_i(y_{cut})$ can be interpreted as the number of events in a $y_{cut}$ bin for which the jet multiplicity changes from $(i+1)$ to $i$. Thus $D_2(y_{cut})$ is just the differential 2-jet rate. $(D_3(y_{cut})-D_2(y_{cut}))$ is equal to the differential 3-jet rate and $(D_4(y_{cut})-D_3(y_{cut}))$ equal to the differential 4-jet rate. For $y_{cut}$ values larger than about 0.04, $D_4(y_{cut})$ is essentially zero, and the differential 4-jet rate is then given by $(-D_3(y_{cut}))$. The $D_i(y_{cut})$ are shown in Fig. 9 and their values listed in Table 4 for the centre of mass energies 14, 22, 35 and 44 GeV. Note that in these distributions the information at which $y_{cut}$ a given event changes its jet multiplicity is used only once. The corrected integrated jet rates $R_2$, $R_3$, $R_4$ and $R_5$ as a function of $y_{cut}$ can be extracted from Table 4 using (8) and the start values $R_i(y_{cut}=0.005)$, $(i=2$–$4)$ which are listed in Table 5.

### *4.4 Simultaneous fit of the scale $\mu^2$ and $\Lambda_{\overline{MS}}$ at all energies*

The theoretical curves were then simultaneously fitted at all centre of mass energies once to all $D_i$-distributions, $(i=2$–$4)$ and once to $D_2(y_{cut})$ and $D_3(y_{cut})$ only. In these fits $\Lambda_{\overline{MS}}$ was treated as a free parameter for various scales $\mu^2$. The change of $\mu^2$ and $\Lambda_{\overline{MS}}$ was handled according to the prescription discussed in Sect. 2 ((1) and (3)). As in Sect. 3 the scale $\mu^2=x\cdot Q^2$ with $0.003\leqq x\leqq 1$ was considered as well as $\mu^2=y\cdot Q^2$ and the set of scales $\mu^2_{opt,2}(y)$ and $\mu^2_{opt,3}(y)$ of [12] for 2- and 3-jet rates, respectively. The results for $\Lambda_{\overline{MS}}$ from the fit of the theory to $D_2(y_{cut})$, $D_3(y_{cut})$ and $D_4(y_{cut})$ at all energies are given in Table 6. Note that these results are valid for the KL′ calculation of the 3-jet cross section. For the distributions entering the fit a finer binning than displayed in Fig. 9 was used. In the fit procedure we started with a bin size of 0.001 and combined those adjacent bins which contained less then 5 entries. The number of degrees of freedom was then 672. The errors are the statistical errors of the fit. Curves representing the fit results for scales $Q^2$, $0.01\cdot Q^2$ and $0.003\cdot Q^2$ are shown in Fig. 9 for the differential rates and also in Fig. 7 for the integrated rates. As found before, the scale $Q^2$ does not describe the data well. It underestimates the 4-jet rate and does not fit the shape of the 3-jet rate. The best fits are achieved with small scales in the range from $0.01\cdot Q^2$ to $0.003\cdot Q^2$*. For such small scales the 2, 3- and 4-jet rates are described in a consistent manner at all energies.

As seen in Figs. 7 and 9, $R_5$ and $D_4$ are not well described by any of the scales. This comes as no surprise since the leading order for these variables is $\alpha_s^3$ and any contributions can come exclusively from effects of the hadronization. For this reason we repeated the fits using only the $D_2(y_{cut})$ and $D_3(y_{cut})$ distributions. These fits gave results consistent with those of Table 6.

As far as the systematic error in the determination of $\Lambda_{\overline{MS}}$ for a given scale is concerned, the dominant contributions come from three sources.

(a) One is the uncertainty in the corrections for massive quarks. We obtain a conservative estimate of the systematic error involved by repeating the analysis entirely without the mass correction. This decreases somewhat the quality of the fit and leads to somewhat lower values of $\Lambda_{\overline{MS}}$. For the scales $0.01\cdot Q^2$ and $0.003\cdot Q^3$ $\Lambda_{\overline{MS}}$ decreases by 5 MeV and 3 MeV, respectively.

(b) The second major contribution to the systematic uncertainties is the dependence of the hadronization correction coefficients $M^i_{kj}$ on the hadronization parameters used in the model. All parameters given in Table 3 were varied within reasonable ranges. The $M^i_{kj}$ were most sensitive to a variation of the mean transverse momentum of mesons introduced in the process of hadronization $\sigma_q$. Varying $\sqrt{2}\cdot\sigma_q$ by 60 MeV typically resulted in a change of $\Lambda_{\overline{MS}}$ of about 13%.

(c) We repeated the fit using bin sizes between 0.001 and 0.01. With increasing bin width the fitted value of $\Lambda_{\overline{MS}}$ was shifted to at most 10% higher values and we account for this uncertainty in the systematic error.

The contributions from these three sources were added in quadrature and are given as the total systematic error on $\Lambda_{\overline{MS}}$. Since we did not study the dependence of our results on the hadronization model used in calculating the corrections we did not consider this source of uncertainty in the systematic error. Summarizing the results of the fit of the differential jet rates one can say that a consistent picture of the data at all energies is

* Note that for the scale $\mu^2=x\cdot Q^2$ the constant $x$ cannot be made arbitrary small. Equation (1) leads to negative values of $\alpha_s$ for very small scales. In the fit this point is reached for $x=0.0025$ and $\Lambda_{\overline{MS}}=60$ MeV at $\sqrt{s}=14$ GeV

obtained for small scales and corresponding values of $\Lambda_{\overline{MS}}$ in the following range.

$$\mu^2 = 0.003 \cdot Q^2 \leftrightarrow 0.01 \cdot Q^2$$
$$\Lambda_{\overline{MS}}[\text{MeV}] = 63 \pm 1.5 \pm 10.6 \leftrightarrow 83 \pm 1.9 \pm 13.8.$$

## 5 Discussion and summary

The 2-, 3- and 4-jet production rates were determined experimentally as a function of the jet resolution $y$ in the energy range of 14 to 44 GeV. They were compared to exact $O(\alpha_s^2)$ QCD calculations, with hadronization taken into account using two different methods. In the comparison both the QCD parameter $\Lambda_{\overline{MS}}$ and the renormalization scale $\mu^2$ were varied.

A strong correlation between $\Lambda_{\overline{MS}}$ and the scale $\mu^2$ was observed. The scale $\mu^2 = Q^2$ leads to large $\Lambda_{\overline{MS}}$ values and to poor overall agreement between data and theory. In particular the 4-jet rate is incorrectly predicted by about a factor of 2. Going to smaller scales improves the description. The coupling constant $\alpha_s$ increases as does the 4-jet rate, which is only calculated to leading order. The increase of $\alpha_s$, however, does not influence the description of the measured 2- and 3-jet rate, since they are formulated renormalization scale invariant up to order $\alpha_s^2$.

Fixing the scale to different values and fitting $\Lambda_{\overline{MS}}$ using the differential jet rates yields a good description of the 2- and 3-jet rate for all scales and results in fitted values of $\Lambda_{\overline{MS}}$ between 269 MeV for $\mu^2 = Q^2$ and 63 MeV for $\mu^2 = 0.003 \cdot Q^2$. The description of the 4-jet rate improves with the reduction of the scale.

A simultaneous fit of $\Lambda_{\overline{MS}}$ and $\mu^2$ leads to small scales in the range from $\mu^2 = 0.003 \cdot Q^2$ to $0.01 \cdot Q^2$. The corresponding $\Lambda_{\overline{MS}}$ values are $\Lambda_{\overline{MS}} = 63 \pm 11$ MeV and $83 \pm 14$ MeV for 5 quark flavours. Note that it is the 4-jet cross section that forces the scale to be small. We conclude that the measured jet cross sections restrict $\Lambda_{\overline{MS}}$ to lie between 63 and 269 MeV, to order $\alpha_s^2$. To get a good description of all the measured jet rates it is necessary to use a small scale $\mu^2$ and a correspondingly small value of $\Lambda_{\overline{MS}}$.

The two methods of treating the hadronization gave consistent results. The small scales needed to describe the data agree well with results obtained by fixing the scale by the method of BLM. Both these scales are of the order of a few GeV$^2$ [35, 36], i.e. below the mass of the bottom quark. Since $\mu^2$ is an unphysical parameter which depends on the order to which the theoretical prediction was calculated, we do not rescale $\Lambda_{\overline{MS}}$ to the number of physical flavours ($N_f = 4$) at this scale.

Our results compare well with other investigations. Aurenche et al. [37] have performed a PMS optimization for the calculation of $\pi^0$ photoproduction in hadron collisions ($\gamma p \to \pi^0 X$). They applied their results to the measurements of the NA14-Collaboration [38] and find $\Lambda_{\overline{MS}} = 120^{+105}_{-50}$ MeV for $N_f = 4$ quark flavours. This can be translated [39] into $\Lambda_{\overline{MS}} = 75^{+75}_{-30}$ MeV for $N_f = 5$ at PETRA energies, in good agreement with our result. Other adjustments of the scale using $e^+e^-$-data have been performed by Bethke [40], the AMY-Collaboration [41], the OPAL-Collaboration [42] and the DELPHI-Collaboration [43]. The results are in agreement with this investigation.

In summary, we find that a small renormalization scale describes the data significantly better than the scale $\mu^2 = Q^2$. The strong dependence of the measured value of $\Lambda_{\overline{MS}}$ on the scale indicates that studies using calculations to higher orders are necessary.

*Acknowledgements.* Helpful discussions with G. Kramer are acknowledged. We are indebted to the PETRA machine group and the DESY computer centre staff for their excellent support during the experiment and to all the engineers and technicians of the collaborating institutions who have participated in the construction and maintenance of the apparatus. This experiment was supported by the Bundesministerium für Forschung und Technologie, by the Ministry of Education, Science and Culture of Japan, by the UK Science and Engineering Research Council through the Rutherford Appleton Laboratory and by the US Department of Energy. The visiting groups at DESY wish to thank the DESY directorate for the hospitality extended to them.

## References

1. JADE-Coll., W. Bartel et al.: Z. Phys. C – Particles and Fields 33 (1986) 23
2. TASSO-Coll., W. Braunschweig et al.: Phys. Lett. B214 (1988) 286
3. T. Sjöstrand: Int. J. Mod. Phys. A3 (1988) 751
4. MARK-II-Coll., A. Petersen et al.: Phys. Rev. D37 (1988) 1, Z. Phys. C – Particles and Fields 43 (1989) 325
5. R.K. Ellis, D.A. Ross, A.E. Terrano: Nucl. Phys. B178 (1981) 421
6. N. Magnussen: Thesis, University of Wuppertal, 1988 (unpublished)
7. G. Kramer, N. Magnussen: DESY-Report, DESY 90-080 (1990)
8. T. Sjöstrand: Comput. Phys. Commun. 39 (1986) 347
9. G. Kramer, B. Lampe: Fortschr. Physik 37 (1989) 181
10. D.W. Duke, R.G. Roberts: Phys. Rep. 120 (1985) 275
11. G. 't Hooft, M. Veltman: Nucl. Phys. B44 (1972) 189
12. G. Kramer, B. Lampe: Z. Phys. C – Particles and Fields 39 (1989) 101
13. G. Kramer: Tracts in Modern Physics, Vol. 102. Berlin, Heidelberg, New York: Springer 1984
14. P.M. Stevenson: Phys. Rev. D23 (1981) 2916
15. S.J. Brodsky, G.P. Lepage, P.B. Mackenzie: Phys. Rev. D28 (1983) 228
16. M.R. Pennington: Durham Univ. Preprint DTP/83/8, (1983)
17. G. Kramer: Proc. of the 1989 Int. Europhysics Conf. on Part. Phys., Madrid 1989
18. F. Gutbrod, G. Kramer, G. Schierholz: Z. Phys. C – Particles and Fields 21 (1984) 235
19. Z. Kunszt: Phys. Lett. 99B (1981) 429
20. K. Fabricius, G. Kramer, G. Schierholz, I. Schmitt: Phys. Lett. 97B (1980) 431; Z. Phys. C – Particles and Fields 11 (1982) 315
21. JADE-Coll., W. Bartel et al.: Phys. Lett. 88B (1979) 171; Phys. Lett. 129B (1983) 145
22. S. Bethke: Habilitationsschrift, Heidelberg (1987) (unpublished)
23. JADE-Coll., S. Bethke et al.: Phys. Lett. 213B (1988) 235
24. JADE-Coll., W. Bartel et al.: Phys. Lett. 115B (1982) 338
25. A. de Rújula et al.: Nucl. Phys. B138 (1978) 387
26. S. Brandt et al.: Phys. Lett. 12 (1964) 37

27. E. Fahri: Phys. Rev. Lett. 39 (1977) 1587
28. G. Hanson et al.: Phys. Rev. Lett. 35 (1975) 1609
29. L. Smolik: Thesis, University of Heidelberg, 1989 (unpublished)
30. B.L. Ioffe: Phys. Lett. 78 B (1978) 277; E. Laermann, P.M. Zerwas: Phys. Lett. 89 (1980) 225
31. G. Kramer, G. Schierholz, J. Willrodt: Z. Phys. C – Particles and Fields 4 (1980) 149
32. JADE-Coll., W. Bartel et al.: Z. Phys. C – Particles and Fields 25 (1984) 231
33. S. Bethke: Z. Phys. C – Particles and Fields 29 (1985) 175
34. S. Bethke: Private communication
35. S. Komamiya: Phys. Rev. Lett. 64 (1990) 987
36. MARK-II Coll., S. Komamiya et al.: Phys. Rev. Lett. 64 (1990) 987
37. P. Aurenche, R. Baier, M. Fontannaz, D. Schiff: Nucl. Phys. B286 (1987) 509; P. Aurenche, R. Baier, A. Douiri, M. Fontannaz, D. Schiff: Nucl. Phys. B286 (1987) 553
38. NA14-Coll., E. Augé et al.: Phys. Lett. 168 B (1986) 163
39. W.J. Marciano: Phys. Rev. D29 (1984) 580
40. S. Bethke: Z. Phys. C – Particles and Fields 43 (1989) 331
41. AMY-Coll., I.H. Park et al.: KEK-Preprint 89-053 (1989)
42. OPAL-Coll., M.Z. Akrawy et al.: Phys. Lett. B235 (1990) 389
43. DELPHI-Coll., P. Abreu et al.: CERN-Preprint CERN-EP 90-89 (1990)